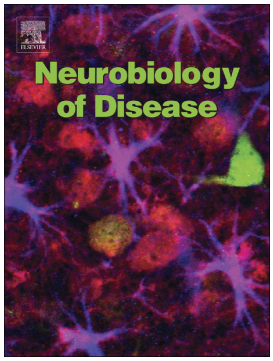

PTEN deletion increases hippocampal granule cell excitability in male and female mice

Victor R. Santos, Raymund Y.K. Pun, Salwa R. Arafa, Candi L. LaSarge, Shane Rowley, Shadi Khademi, Tom Bouley, Katherine D. Holland, Norberto Garcia-Cairasco, Steve C. Danzer

PII: S0969-9961(17)30204-8
DOI: doi: 10.1016/j.nbd.2017.08.014
Reference: YNBDI 4023

To appear in: *Neurobiology of Disease*

Received date: 2 June 2017
Revised date: 10 August 2017
Accepted date: 26 August 2017

Please cite this article as: Victor R. Santos, Raymund Y.K. Pun, Salwa R. Arafa, Candi L. LaSarge, Shane Rowley, Shadi Khademi, Tom Bouley, Katherine D. Holland, Norberto Garcia-Cairasco, Steve C. Danzer , PTEN deletion increases hippocampal granule cell excitability in male and female mice, *Neurobiology of Disease* (2017), doi: 10.1016/j.nbd.2017.08.014

PTEN deletion increases hippocampal granule cell excitability in male and female mice

Victor R. Santos*[1,2], Raymund Y.K. Pun*[1], Salwa R. Arafa[1,5], Candi L. LaSarge[1], Shane Rowley[1], Shadi Khademi [1], Tom Bouley[1], Katherine D. Holland[4], Norberto Garcia-Cairasco[2], and Steve C. Danzer[1,3]

[1]Department of Anesthesia, Cincinnati Children's Hospital Medical Center, Cincinnati, OH, 45229

[2]Department of Physiology, Ribeirão Preto Medical School, University of São Paulo, Ribeirão Preto-SP, Brazil

[3]Departments of Anesthesia and Pediatrics, University of Cincinnati, Cincinnati, OH, 45267

[4]Division of Neurology, Cincinnati Children's Hospital Medical Center, Cincinnati, OH, 45229

[5]University of Cincinnati, College of Pharmacy, Cincinnati, OH 45267

*These authors contributed equally to this work.

Corresponding author:

Dr. Steve C. Danzer

3333 Burnet Avenue, ML 2001

Cincinnati, Ohio 45229-3039

(513) 636-4526 (phone)

Email: steve.danzer@cchmc.org

Running Title: PTEN regulates neuronal excitability

Number of Pages: 42

Number of Figures: 8

Number of Tables: 0

Conflicts of Interest: Nothing to report

Acknowledgements

We thank Dr. Lili Ding (CCHMC) for help with statistical analyses and Keri Kaeding for editorial advice on the manuscript. We thank the CCHMC Confocal Core for providing access to the Nikon microscopes used in this study.

Funding

This work was supported by the National Institute of Neurological Disorders and Stroke (SCD, Award Numbers R01NS065020 and R01NS062806). VRS received a Fellowship from the Coordenação de Aperfeiçoamento de Pessoal de Nível Superior (CAPES) Brazil. His work, under the mentorship of SD at CCHMC, was part of his PhD Program at the University of São Paulo, Brazil. The content is solely the responsibility of the authors and does not necessarily represent the official views of the National Institute of Neurological Disorders and Stroke or the National Institutes of Health.

Abstract

Deletion of the mTOR pathway inhibitor PTEN from postnatally-generated hippocampal dentate granule cells causes epilepsy. Here, we conducted field potential, whole cell recording and single cell morphology studies to begin to elucidate the mechanisms by which granule cell-specific PTEN-loss produces disease. Cells from both male and female mice were recorded to identify sex-specific effects. PTEN knockout granule cells showed altered intrinsic excitability, evident as a tendency to fire in bursts. PTEN knockout granule cells also exhibited increased frequency of spontaneous excitatory synaptic currents (sEPSCs) and decreased frequency of inhibitory currents (sIPSCs), further indicative of a shift towards hyperexcitability. Morphological studies of PTEN knockout granule cells revealed larger dendritic trees, more dendritic branches and an impairment of dendrite self-avoidance. Finally, cells from both female control and female knockout mice received more sEPSCs *and* more sIPSCs than corresponding male cells. Despite the difference, the net effect produced statistically equivalent EPSC/IPSC ratios. Consistent with this latter observation, extracellularly evoked responses in hippocampal slices were similar between male and female knockouts. Both groups of knockouts were abnormal relative to controls. Together, these studies reveal a host of physiological and morphological changes among PTEN knockout cells likely to underlie epileptogenic activity.

Significance Statement

Hyperactivation of the mTOR pathway is associated with numerous neurological diseases, including autism and epilepsy. Here, we demonstrate that deletion of the mTOR negative regulator, PTEN, from a subset of hippocampal dentate granule impairs dendritic patterning, increases excitatory input and decreases inhibitory input. We further demonstrate that while granule cells from female mice receive more excitatory and inhibitory input than males, PTEN deletion produces mostly similar changes in both sexes. Together, these studies provide new insights into how the relatively small number (≈200,000) of PTEN knockout granule cells instigates the development of the profound epilepsy syndrome evident in both male and female animals in this model.

Introduction

During the development of temporal lobe epilepsy, adult-generated dentate granule cells integrate abnormally into the hippocampus (Shapiro et al., 2007; Walter et al., 2007; Jessberger and Parent, 2015; Singh et al., 2016; Althaus et al., 2016). Abnormal granule cells are hypothesized to mediate epileptogenesis by impairing the "dentate gate", a property of the hippocampal circuit that normally limits excess excitation (Krook-Magnuson et al., 2015; Scharfman and Bernstein, 2015). Supporting this hypothesis, genetic ablation of abnormal, newborn granule cells reduces epilepsy severity (Cho et al., 2015; Hosford et al., 2016). To further test the hypothesis, we deleted the mechanistic target of rapamycin (mTOR) pathway inhibitor phosphatase and tensin homologue (PTEN) from a subset of postnatally-generated granule cells. PTEN deletion from granule cells produces axonal and dendritic abnormalities reminiscent of those seen in epilepsy (Kwon et al., 2006; Murphy et al., 2012; LaSarge and Danzer, 2014; LaSarge et al., 2015) and leads to the development of spontaneous seizures; demonstrating that abnormal granule cells can cause epilepsy (Pun et al., 2012).

PTEN mutations are associated with a number of neurological conditions, including megalocephaly, autism spectrum disorder and epilepsy (O'Roak et al., 2012; Garcia-Junco-Clemente and Golshani, 2014; Jansen et al., 2015). PTEN-induced hyperactivation of the mTOR pathway mediates many of the abnormalities evident in animal models (Kwon et al., 2003; Zhou et al., 2009; Nguyen et al., 2015; Matsushida et al., 2016). mTOR is a major target of the PI3K-Akt pathway, activating signaling cascades that regulate neuronal proliferation, survival, growth and plasticity (Switon et al., 2017). Aptly-named mTORopathies – diseases associated with altered mTOR signaling – cover an even broader range of neurological conditions, including

neurocognitive and neurodegenerative disorders (Lipton & Sahin 2014; Crino, 2016). In addition to genetic mutations which dysregulate mTOR signaling, the mTOR pathway is also hyperactivated in granule cells following neuronal injuries associated with acquired epilepsies, and blocking mTOR signaling is anti-epileptogenic in most (Zeng et al., 2009; Huang et al., 2010; Butler et al., 2015) but not all (Heng et al., 2013) epilepsy models that have been examined.

The model used for the present study, therefore, allows us to explore the impact of deleting an epilepsy-associated gene (PTEN) from a neuronal population (granule cells) hypothesized to play a critical role in temporal lobe epilepsy. We also use this model to gain insight into sex differences in epilepsy. Steroid hormones play a key role in the control of neuronal excitability. Estradiol potentiates glutamatergic synaptic transmission, increases presynaptic glutamate release probability and enhances postsynaptic sensitivity in both sexes (Wong and Moss, 1992; Oberlander and Woolley, 2016). By contrast, exposure to estradiol can suppress GABAergic inhibition of hippocampal neurons (Huang and Woolley, 2012). Consistent with these findings, estradiol can impact seizure susceptibility (Scharfman and MacLusky, 2014; Reddy, 2017). In addition, several studies have identified sex difference in mTOR signaling in non-CNS tissues and functions (Gürgen et al., 2013; Miller et al., 2014; Baar et al., 2016).

Here, neuronal function was assessed using both extracellular and intracellular recording techniques, combined with detailed cellular morphometry. Findings provide new insights into the mechanisms by which a relatively small population of abnormal neurons, in the absence of a

precipitating injury producing widespread cell loss, lead to convulsive seizures affecting much of the brain.

Methods

All animal procedures were conducted in accordance with NIH and CCHMC Institutional Animal Care and Use Committee (IACUC) guidelines. To generate study animals, Gli1-CreER^{T2} (RRID:IMSR_JAX:007913) hemizygous::PTEN$^{wt/flox}$ (RRID:IMSR_JAX:006440) mice were crossed to PTEN$^{wt/flox}$ mice to generate Gli1-CreER^{T2} hemizygous::PTEN$^{flox/flox}$ mice (male PTEN KO, n=24; female PTEN KO, n=15). Gli1-CreER^{T2} hemizygous::PTEN$^{wt/wt}$ and Gli1-CreER^{T2} negative::PTEN$^{wt/wt,\ flox/wt\ and\ flox/flox}$ littermates were used as controls (male control, n=14; female control, n=10). PTEN KO mice were injected with tamoxifen on P14 (Sigma-Aldrich, T5648; 250 mg/kg dissolved at 20 mg/ml in corn oil, subcutaneous). Thirteen of 24 control mice also received tamoxifen. Within controls, tamoxifen injection did not significantly impact any measure presented (data not shown), so groups were merged. Animals ranged in age from 2-6 months, with median ages of 3.4 (male controls), 3.6 (female controls), 3.0 (male KOs) and 3.0 (female KOs) months (one-way ANOVA, p=0.783). Most seizures in these animals are non-convulsive (Pun et al., 2012), so animals were not video-monitored to assess seizure frequency. Power analyses to determine target "n's" were not conducted due to a lack of pilot data for most measures. Therefore, historical targets of 5-8 cells/groups were used, although larger "n's" were generated for most measures to offset experimental noise that might result from variable seizure rates.

Slice preparation

Hippocampal slices were prepared for physiological recordings as follows. Mice were anesthetized with pentobarbital (i.p., 0.05 ml, 100 mg/ml) and perfused intracardially with ice-cold modified ACSF of the following composition (mM): NaCl, 92; KCl, 2.5; $NaH2PO_4$, 1.25; $NaHCO_3$, 30; $MgSO_4$, 10; $CaCl_2$, 0.5; Na-pyruvate, 3; Thiourea, 2; Na-ascorbate, 5; Glucose, 25; HEPES, 20. ACSF was oxygenated with 95% O_2/5% CO_2. The brain was removed and bisected. A tissue slicer (Campden/Lafayette Instrument, IN) was used to prepare 350 μm thick transverse slices from the right hemisphere for physiological recordings, as described by Jones and Heinemann (1988). Individual slices were transferred to a N-methyl-D-glutamine (NMDG)-based medium with the same composition as ACSF, except that NaCl was replaced with NMDG (92 mM). Slices were equilibrated in oxygenated NMDG-based medium for 60 minutes at room temperature. The modified ASCF and NMDG solutions better preserve physiological responses from older animals (Zhao et al., 2011; Althaus et al., 2015). After the first incubation, the slices were transferred into recording ACSF for another 60 minute incubation. Recording ACSF was of the following composition and concentration (mM): NaCl, 124; KCl, 3.5; $MgSO_4$, 2; $CaCl_2$, 2; NaH_2PO_4, 1.25; glucose, 10; $NaHCO_3$, 26. Individual slices were placed in a chamber on the stage of an upright microscope (Nikon, Eclipse FNI) equipped with a 10X bright field and a 40X DIC objectives, and continuously perfused with oxygenated ACSF at a rate of 3-4 ml/minute at room temperature.

Extracellular recordings

A stimulating electrode, mounted on the stage of the microscope, was used to activate the perforant pathway. The electrode was constructed from a sharp-tipped tungsten wire (impedance

approximately 1-2 Mohm; FHC, Maine) and a stainless steel wire -- each placed through one barrel of a 6 cm long double-barreled glass pipette. The pipette was sealed at the end with Sylgard, with the exposed wire tips separated by 50-75 µm. Responses were elicited by a 200 µsec 4-8 V step, generated by the D/A interface and timed by Clampex software (version 10.3; Molecular Devices).

To provide a measure of excitability in slices, extracellular evoked potentials were classified as consisting of 1) isolated excitatory postsynaptic potentials (EPSPs), 2) an EPSP + a single population spike, 3) an EPSP + multiple asynchronous population spikes and 4) an EPSP + multiple synchronous population spikes. EPSPs were defined as an initial peak occurring within 5 msec of the stimulus artifact, with an exponential decay. Population spikes were defined as negative deflections following the EPSP with an amplitude at least five times greater than baseline. Multiple, asynchronous population spikes were defined as occurring when two or more secondary spikes appeared with variable latency (> 10 ms) following a single stimulation of the perforant path. Multiple, synchronous population spikes were defined as two or more spikes which occurred with identical latencies between trials. A minimum of four stimulation trials at 6V was used to assess responses. Responses were assigned scores of 1-4 (as above), providing a semi-quantitative measure of excitability for statistical comparisons. Higher scores suggest increased excitability.

Intracellular recordings

Intracellular recording electrodes were fabricated from thin-walled borosilicate glass pipettes (O.D., 1.5 mm; I.D., 1.12 mm) using a computer controlled BB-CH-PC micropipette puller (Mecanex, Switzerland). Electrodes were filled with a solution composed (in mM) of

Kgluconate, 135; KCl, 5; NaCl, 5; EGTA, 5; HEPES, 10, $MgCl_2$, 2; glucose, 10 supplemented with 2 mM ATP and 200 µM GTP (free Ca^{2+} level is estimated to be below 10 nM). This solution had a pH of 7.2 and an osmolarity between 290-295 mOs. Electrode resistance was 6-7 Mohms. Current and voltage recordings were made with an Axopatch 200B amplifier (Molecular Devices) controlled by Clampex software (version 10.3) with a Digidata interface (Model 1440, Molecular Devices). Results were analyzed with Clampfit (version 10.3). All extracellular solutions used had a pH between 7.3 and 7.4, osmolarity of 295-305 mOs (adjusted by addition of sucrose) and were continuously aerated with a mixture of 95% O_2/5% CO_2. All experiments were carried out at room temperature unless otherwise stated.

Voltage clamp experiments were conducted at a holding potential of -70 mV. Voltage ramps from -100 mV to +40 mV, duration 1 sec at 0.1-0.2 Hz were used to generate ramp currents unless otherwise stated. At least 6 ramps were used for each run. The current recorded during the voltage ramp reflects the I-V relationship of the cells and allows for the estimation of the input resistance (Pun and Kleene; 2003, 2004). Several membrane parameters were determined from the ramp, including: 1) the input resistance of the cell, obtained from the slope of the linear regression fit to the "subthreshold" region of the I-V relation (between -80 and -50 mV and prior to the generation of the rapidly inactivating inward or action potential current (spike)); 2) the spike (or activation) threshold, which is the voltage at which the first spike is generated; 3) the peak inward amplitude of the 1st spike elicited and 4) the peak outward current at the end of the 1st ramp. Membrane parameter measurements were excluded if there was a positive shift in the activation potential and a reduction in peak spike currents between the first 2 runs (1 minute apart); changes likely reflecting a shift in access or series resistance. Access

resistance (range 6-16 mohm) was not compensated in our studies. Cells were excluded if the holding current was larger than -100 pA.

Spontaneous excitatory synaptic currents (sEPSCs) were recorded at a holding potential of -70 mV. At least three, 30-second data files (90 seconds total) were used to obtain the frequency of excitatory synaptic currents for each cell; although for most cells a total of 6-10 files (3-5 minutes) were used for EPSCs. Spontaneous inhibitory currents (sIPSCs) were obtained at -40 mV to -30 mV. At least six, 30 second data files (180 seconds total) were used for IPSCs analyses. Longer recordings compensate for noisier baselines at more positive holding potentials, and the presence of sEPSCs, which can obscure sIPSCs. sEPSC/sIPSC ratios were obtained for individual cells when possible.

Reconstruction of cell morphology

To obtain the morphology of recorded cells 0.2% biocytin was included in the recording pipette solution. At the end of a recording session, slices were put into fixative (2.5% paraformaldehyde, 4% sucrose in 0.1M phosphate-buffered saline [PBS]) and left overnight. The next day, slices were rinsed in PBS for 15 minutes, exposed to 0.5% Igepal in PBS for one hour, followed by a 2 hour incubation in streptavidin-Alexa Fluor® 488 conjugate (Molecular Probes Cat# S32354 also S32354 RRID:AB_2315383) at room temperature. Slices were mounted with ProLong® Gold Antifade Mountant (Molecular Probes, Life Technologies, Cat# P10144). Cells were imaged with a Nikon A1Rsi inverted microscope equipped with a 40x water objective (NA=1.15). 3-dimensional stacks were collected through the z-depth of the tissue at 0.5 µm increments to capture cells in their entirety. Multiple image stacks were required to capture

neurons with sufficient resolution, so overlapped image stacks were three-dimensionally montaged into a single image using Neurolucida software (Microbrightfield Inc., RRID:SCR_001775). These montages were used to digitally reconstruct the neurons by an observer unaware of animal or cell groups. Reconstructions encoded soma area, apical and basal dendrite length, and dendritic branch points. Image stacks were also used to encode the location of the hilar-granule cell body layer border, the granule cell body layer–molecular layer border, and the location of the hippocampal fissure. The molecular layer was further subdivided into inner (IML), middle (MML), and outer (OML) regions, with the inner region being the first 17% of the molecular layer (West and Andersen, 1980; Deller et al., 1999; van Groen et al., 2003; Danzer et al., 2004; Murphy et al., 2011), and the middle and outer being an equal split of the remainder. These subdivisions are only approximate, however, because exact divisions between layers are not clearly discernible.

Immunohistochemistry, cell counting and soma measurements

The right half of the brain was used to prepare slices for electrophysiological recordings. After bisection of the brain, the left hemisphere was immediately put into fixative (2.5% paraformaldehyde, 4% sucrose in PBS), fixed overnight, cryoprotected in 10%, 20%, 30% sucrose in PBS each for a minimum of 24 h. Half-brains were snap-frozen in 2-methylbutane chilled to -25 to -40°C with dry ice and stored at -80°C until sectioning. Half-brains were sectioned sagittally at 60 µm using a cryostat maintained at -20°C. Sections were mounted to glass slides and air dried for <1 hour before storing at -80°C.

Sections were immunostained with 1:250 rabbit anti-PTEN (Cell Signaling Technology Cat# 9559 also 9559L RRID:AB_390810) primary antibodies, followed by 1:750 goat anti-rabbit Alexa Fluor 555 (Thermo Fisher Scientific Cat# A27039 RRID:AB_2536100) secondary antibodies. Sections were counter stained with NeuroTrace® 640/660 Deep-Red Fluorescent Nissl Stain (Thermo Fisher Scientific Cat# N21483 RRID:AB_2572212). After staining, sections were dehydrated in serial alcohol washes, cleared in xylenes, and hard mounted with Krystalon (EMD Millipore, Cat# 64969). Use of PTEN/Nissl co-staining was validated against our previous protocol using PTEN/NeuN to identify knockout granule cells (Pun et al., 2012; LaSarge et al., 2015; 2016), and found to be equally effective (data not shown).

Images of PTEN/Neurotrace-labelled sections were collected using a Nikon A1GaAsP confocal microscope using a 40X water objective (Apo LWD 40X WI λS DIC N2, NA=1.15, field dimension= 1024 X 1024, 0.31 µm/px). Confocal image stacks (15 µm depth, 1 µm z-step) were collected from upper and lower blades of the dentate gyrus from sections at the same medial-lateral coordinates (Lateral 1.56; Paxinos and Franklin, 2001) for each animal. Image stacks were imported into Neurolucida software and 100 X 100 µm counting frames were placed over the midpoints of the upper and lower blades of the dentate gyrus. Frames encompassed the entire width (hilar to molecular layer border) of the dentate gyrus. The top section of the z-stack, and the top and right sides of the frame were set as exclusion zones. Cells crossing any one of these three planes were not counted. Remaining cells within the frame were identified as either Neurotrace+, PTEN+ cells, or Neurotrace+, PTEN- cells. Neurotrace labels both neurons and glia, but since the tightly packed granule cell layer contains almost exclusively granule cells, the small number of glia and non-granule cell neurons included in the counts is negligible. The

percentage of PTEN knockout granule cells was obtained by dividing the number of PTEN- cells by the total number of Neurotrace+ cells within the 2 squares. Neurolucida software was also used to measure the soma area of PTEN+ granule cells from control animals, and PTEN- and PTEN+ cells from knockout animals.

Statistics

All measurements were conducted by an investigator blind to treatment group and cell genotype. Results are presented as mean ± s.e.m. or medians [25-75% interquartile range]. Statistical tests were performed using Sigma Plot software (version 13.0, Systat Software, Inc., San Jose, CA, RRID:SCR_003210). Two-way ANOVA's with Holm-Sidak post-tests were used for data that met assumptions for normality and equal variance. Data that failed either test were normalized using rank or square root transformations. Given the dependence between observations from the same animal, analysis of repeated measures was carried out. Linear mixed effect models were used for continuous outcomes; Poisson mixed effects model for count data and logistic mixed effects model for binary outcome, with cell genotype and sex as predictors and random animal effects. SAS software (version 9.3, SAS Institute Inc., Cary, N.C.; RRID:SCR_008567) was used for these analyses. Specific tests were used as noted in the results. Alpha was set at $p < 0.05$. In many cases, it was not possible to collect every measure from every cell recorded due to technical issues (e.g. patch electrode seal broke), so sample size "n" is reported for each result.

Image preparation

Confocal images for figures were generated using NIS-Elements software (version 4.50.00, Nikon). Images in figures 4 and 5 are neuronal reconstructions (McAuliffe et al., 2011; Santos et al., 2011; Singh et al., 2016). Figures were prepared using Adobe Photoshop CS5 (version 12.0, Adobe Photoshop; RRID:SCR_014199). Images were adjusted to enhance brightness and contrast. Identical adjustments were made to images meant for comparison.

Results

Identification of PTEN knockout cells in tissue with mosaic gene deletions

All PTEN knockout (KO) animals used in the present study are mosaics, with PTEN knockout cells adjacent to cells with intact PTEN expression (Fig.1). We first ascertained the percentage of KO cells in male and female mice. We have previously shown that the phenotype increases in severity with more KO cells (Pun et al., 2012), so this is an important variable. The percentage of granule cells lacking PTEN was identical between male and female PTEN KO mice (male, n=15, 26.7±1.4% [range 19.1-34.1]; female, n=7, 26.7±2.7% [range 14.9-36.5], t-test, p=0.989). Our prior work indicates that animals with >10% KO cells develop epilepsy in this model (Pun et al., 2012), so animals in the present study are predicted to be epileptic.

No attempt was made to distinguish between PTEN-expressing and PTEN KO cells during whole cell recordings. Cells were identified and grouped only after histological analyses were complete. Soma area of biocytin filled cells was used to distinguish PTEN KO from PTEN-expressing cells. PTEN deletion has been consistently demonstrated to induce a dramatic increase in soma area (Fig.1; Kwon et al 2001, 2003, 2006; Ljungberg et al., 2009; Amiri et al 2012; Williams et al 2015). For the present study, KO cells were defined as cells with soma areas two standard deviations larger than the mean soma area of cells from male and female control animals (male control, 114.8±11.3 μm^2, [mean±SD]; female control, 101.8 ± 20.0 μm^2). Studies examining soma area in tissue double-immunostained for NeuN and PTEN confirmed that this approach effectively segregates PTEN KO from PTEN-expressing cells with >95% sensitivity and specificity (Fig.1, graph; n=30 cells from 3 control mice [10 cells/mouse], plus 80 PTEN-immunonegative and 86 PTEN-immunopositive cells from 8 PTEN KO mice [≥10 cells/mouse]).

For the present study, only PTEN KO cells and cells from control animals are included; PTEN-immunopositive cells from KO mice are not included.

PTEN KO cells exhibit altered membrane properties

Median input resistance was decreased for PTEN KO cells from both male and female mice relative to male and female controls (male control, n=21 cells, 422 Mohm [384-565]; male KO, n=35, 213 Mohm [160-250]; female control, n=15, 439 Mohm [374-580]; female KO, n=19, 200 Mohm [153-238]; $p<0.001$, linear mixed effect model). Male and female control and KO cells were statistically identical to each other, respectively ($p=0.721$). Decreased input resistance likely reflects, at least in part, the increased soma area of KO cells, assuming the density of channels responsible for the "resting" conductance is not changed. Action potential threshold was similar in cells from male (control, n=19, -41.1 ± 2.3 mV; KO, n=24, -42.0 ± 2.0 mV) and female (control, n=14, -44.8 ± 2.7 mV; KO, n=18 -44.5 ± 2.3 mV) mice for both cell genotype ($p=0.881$) and sex ($p=0.189$, two way ANOVA). Peak inward currents (male control, n=21, -1038 pA [-1770 to -722]; male KO, n=37, -691 pA [-1099 to -506]; female control, n=15, -1249 pA [-1533 to -498]; female KO, n=21, -1041 pA [-1536 to -659]; $p=0.757$ for genotype, $p=0.578$ for sex, linear mixed effects model) and peak outward currents measured at the end of the ramp (male control, n=19, 972 pA [556-1587]; male KO, n=23, 807 pA [709-1095]; female control, n=14, 800 pA [579-1103]; female KO, n=18, 856 pA [720-1287]; $p=0.465$ for genotype, $p=0.283$ for sex, linear mixed effects model) were indistinguishable among the groups. Similar inward and outward currents suggest that sodium and potassium conductances at the soma, respectively, are not dramatically altered.

PTEN KO cells exhibit a tendency towards burst firing

PTEN KO cells exhibited an unusual propensity to fire doublets or triplets during the initial response to a voltage ramp (Fig.2). To quantify this effect, we measured the interval between the first and second action potential currents (spikes) initiated by the ramp. Median spike intervals were 34 [30-42] ms for male controls (n=21), 16 [12-49] ms for male KOs (n=36), 33 [31-41] ms for female controls (n=15) and 13 [11-50] ms for female KOs (n=21). The interspike interval was significantly shorter for KO cells relative to control cells ($p=0.005$, two-way ANOVA on ranked data). No differences between male and female groups were found ($p=0.996$).These data were also analyzed by categorizing cells as either firing doublets if the interspike interval was 16 ms or less, or not firing doublets for longer interspike intervals. When examined in this fashion, 0% of male and female control cells fired doublets (males, 0 of 21; females, 0 of 15) while 52.8% (19 of 36) of male KO cells and 57.1% (12 of 21) of female KO cells fired doublets ($p<0.001$, z-test, males and females combined within genotype).

PTEN KO cells from males show reduced inter-spike frequencies

The occurrence of doublets and triplets produces very short interspike intervals for the first few spikes. To gain a better picture of the entire response, however, we also quantified interspike intervals for spikes occurring after the initial voltage ramp-induced burst. Only cells that had four or more such spikes were used to obtain interspike intervals, with measurements beginning with the first spike after the burst (if present). Interestingly, a significant interaction between sex and genotype was found ($p=0.047$, two-way ANOVA on ranked data; male control, n=18; male KO, n=26; female control, n=12; female KO, n=18). Inter-spike intervals were significantly longer for male KO cells relative to male control cells (Fig.2; $p<0.001$, Holm-

Sidak). Intervals were statistically identical between female control and KO cells (p=0.415). Despite frequent initial bursts of high frequency firing among male KO cells, therefore, subsequent firing occurred at lower frequencies.

We also measured the number of spikes generated during voltage ramps to assess the cells ability for sustained firing. Overall, male and female KO cells exhibited significantly more spikes than male and female control cells (Fig.2; p=0.008, two-way ANOVA on sq. rt. transformed data). A non-significant trend for an interaction between sex and genotype was also observed (p=0.067). The trend was driven by a 26% increase in female KOs, while male KOs exhibited only a modest 4.6% increase.

PTEN KO cells exhibit increased sEPSCs frequency, and reduced sIPSC frequency

Since PTEN deletion increases dendritic spine density (Pun et al., 2012), we queried whether spontaneous excitatory postsynaptic current (sEPSC) frequency would show a corresponding increase. PTEN deletion led to a significant increase in sEPSC frequency among cells from both male (n=23) and female (n=12) KO mice relative to cells from male (n=14) and female (n=9) controls (Fig.3; p<0.001; two-way ANOVA on square root transformed data with Holm-Sidak post-test). Moreover, a significant effect of sex was found (p=0.005), with females having higher sEPSC frequencies than males. No interaction between genotype and sex was found (p=0.599).

Exacerbating the increase in sEPSC frequency, cells from PTEN KO mice exhibited a decrease in spontaneous inhibitory postsynaptic current (sIPSC) frequency relative to controls.

Frequency was significantly decreased for cells from both male (n=21) and female (n=10) KO mice relative to cells from male (n=9) and female (n=10) controls (Fig.3; Two-way ANOVA with Holm-Sidak post-tests, $p<0.001$). Interestingly, however, a significant sex effect was also found, with cells from female mice (both controls and KOs) showing higher sIPSC frequencies ($p=0.042$ for different levels of sex, no interaction between sex and genotype, $p=0.778$). The higher frequency of sIPSCs potentially offsets the higher sEPSC frequencies evident among females. Consistent with this interpretation, the sEPSP/IPSP ratio did not differ between males and females ($p=0.217$), although the ratio was significantly increased between control and KO mice (Two-way ANOVA, $p<0.001$).

PTEN KO cells exhibit increased dendrite length and branching

Recorded cells were filled with biocytin for morphological characterization (Fig.4). KO cell soma area was statistically identical in male and female mice (male KO, 213 μm^2 [172-227]; female KO, 187 μm^2 [162-246]; $p=0.525$, Mann-Whitney Rank Sum Test). The number of primary apical dendrites was increased among male and female KO cells relative to controls (male control, n=13, 2 primary dendrites [1-2]; male KO, n=29, 2 [2-3]; female control, n=11, 1 [1-2]; female KO, n=17, 2 [2-3.5], $p<0.0001$; Overdispersed Poisson model), but KO cells from males and females did not differ ($p=0.8830$). Total dendrite length was significantly increased among cells from male (n=28) and female (n=16) KO mice relative to male (n=13) and female (n=11) controls (Fig.5; $p<0.001$, two-way ANOVA on ranked data with Holm-Sidak post-test). Dendrite length was similar between the sexes ($p=0.982$). To explore whether altered granule cell apical dendrite length is specific to regions receiving distinct afferent inputs, dendritic trees were subdivided into segments contained within the granule cell layer, or inner, middle and outer

molecular layers. For KO cells from both male and female animals, PTEN deletion increased dendrite length in the granule cell layer ($p<0.001$, two-way ANOVA on ranked data) and inner molecular layer ($p<0.026$, linear mixed effects model), while a trend towards increased length was evident in the outer molecular layer ($p=0.078$, two-way ANOVA). No change was evident in the middle molecular layer for either genotype ($p=0.555$, two-way ANOVA). No effect of sex was found for either the granule cell layer ($p=0.571$, two-way ANOVA on ranked data), inner ($p=0.713$, mixed effects model), middle ($p=0.368$, two-way ANOVA) or outer ($p=0.654$, two-way ANOVA) molecular layer (Fig.5).

The median number of branches per apical dendrite tree increased by more than 50% for male (n=26) and female (n=18) KO cells relative to male (n=11) and female (n=11) controls (Fig 6; $p<0.001$; Poisson mixed effects model). Males and females, however, were statistically identical within treatment groups ($p=0.340$). When examined by layer (Fig 5), the number of branch nodes was similar between controls and KOs in the dentate granule cell layer ($p=0.120$, Poisson mixed effects model) and middle molecular layer ($p=0.186$, Poisson mixed effects model), but was modestly increased in the inner molecular layer ($p=0.011$, Poisson mixed effects model). The most striking increase, however, was observed in the outer molecular layer, where the number of nodes increased more than 700% for male and female KO cells relative to controls ($p<0.0001$, zero inflated Poisson model). Males and females did not differ from each other in any of the regions (DGC-L, $p=0.503$; IML, $p=0.811$; MML, $p=0.737$; OML, $p=0.364$).

PTEN KO cells exhibit abnormal morphology

Dendritic tree structure was grossly abnormal for PTEN KO cells (Fig.6), with many cells exhibiting a collapsed or "closed parasol deformation" of their dendritic trees (Scheibel and Scheibel, 1973), indicative of the failure of the cells to distribute their branches evenly in space (Fig.4). To quantify this effect, we calculated the number of times dendritic branches crossed each other in two-dimensional projections (Fig.7A), creating a "dendritic overlap" index. Dendritic overlap was dramatically increased among male (n=26) and female (n=14) PTEN KO cells relative to male (n=12) and female (n=8) controls ($p<0.001$; two way ANOVA on ranked data), but males and females did not differ from each other ($p=0.941$).

As an additional measure of dendritic field structure, we conducted 3D convex hull analyses. Briefly, the convex hull can be imagined as a rubber sheet wrapped around each primary dendrite of the cell. The volume encased by the sheet provides a numerical value for the amount of neuropil than can potentially be sampled by that dendritic tree. For each cell, 3D convex hull values were calculated for each primary dendrite and then summed for the cell. Despite the increase in total dendritic length among KO cells, convex hull volumes were similar among groups (Fig.7B; male control, n=13; male KO, n=28; female control, n=11; female KO, n=18, $p=0.405$; two way ANOVA on sq. root transformed data) and males and females did not differ ($p=0.482$). We next calculated the average volume per primary dendrite, revealing a significant decrease for KO cells relative to controls (Fig.7C; $p=0.023$; two way ANOVA on ranked data). Males and females did not differ ($p=0.910$). These data indicate that while KO cells have more primary dendrites, each individual primary dendrite samples a smaller volume of neuropil. Finally, we divided total dendritic hull volume per cell by the total dendritic length for

each cell, giving an estimated volume for each micron of dendrite. KO cells exhibited a non-significant decline in volume per micron of dendrite (Fig.7D; two way ANOVA; male vs. female, p=0.379). In summary, therefore, control and KO cells have the potential to sample similar volumes of neuropil, however, KO cells achieve this with significantly more primary dendrites and significantly longer dendritic trees (Fig.7E), likely reducing their sampling efficiency and producing the apparent increase in dendritic overlap evident in 2D projections.

Basal dendrite formation among PTEN KO cells

In addition to abnormal apical dendritic trees, the majority of PTEN KO cells also developed elaborate hilar basal dendrites (Fig. 4). KO cells from male (n=27) and female (n=17) animals had medians of one and two spiny basal dendrites/cell, respectively [range, 0-4 for males and 0-3 for females]. Basal dendrites were absent from male (n=13) and female (n=11) control cells ($p<0.01$, male and female KOs vs controls, respectively; one-way ANOVA with Dunn's post-test). Median basal dendrite number (p=0.425, Mann-Whitney rank sum test) and length (male KO, 113.8 μm [0.0-713.9]; female KO, 138.6 μm [0.0-785.0]; p=0.623, rank sum test) were statistically similar among KO cells from male and female mice.

Recent work suggests that axons which originate from a basal dendrite, rather than the soma, convey distinct properties to the parent cell (Thome et al., 2014; Kelly and Beck, 2017). We queried, therefore, the extent to which KO cells exhibit basal dendrite-originating axons. Forty percent (6 of 15) of KO cells from female mice, and 25% of KO cells from male mice (7 of 28) had basal dendrite-originating axons. The incidence did not differ significantly between males and females (p=0.501, z-test).

Male and Female PTEN KO mice show identical abnormalities at the network level

Physiological and morphological studies reveal mostly identical abnormalities between KO cells from male and female mice, with the increase in interspike interval being a notable exception for male KO cells. Both male and female KO cells showed changes indicative of increased excitability. Given these observations at the single cell level, we queried whether they would hold at the network level.

Field potential responses were evoked from hippocampal slices from control and PTEN KO mice. In control slices, stimulation of the perforant path reliably evoked excitatory postsynaptic potentials, which were often followed by a population spike recorded in the granule cell body layer. By contrast, PTEN deletion enhanced the input/output curve and led to the appearance of multiple secondary population spikes, consistent with prior findings (Takeuchi et al., 2013; LaSarge et al., 2016). Repeated stimulations of the same slice revealed two patterns of secondary spikes; either asynchronous, with secondary spikes appearing at variable intervals following the stimulus artifact, or synchronous, with secondary spikes always appearing with the same latency. These criteria were used to establish the following semi-quantitative scale for scoring responses: 1) EPSP only; 2) EPSP + population spike; 3) EPSP + multiple asynchronous population spikes and 4) EPSP + multiple synchronous population spikes (Fig.8). With this scale, slices from male (n=13) and female (n=7) control animals received median scores of 1.0 [1.0-1.5] and 1.0 [1.0-2.0], respectively. Male (n=18) and female (n=10) knockout animals received scores of 3.0 [2.4-4.0] and 3.5 [2.8-4.0], respectively. Male and female knockouts differed significantly from controls (Fig.8; $p<0.0001$, linear model), but not from each other

(p=0.5505). The absence of a circuit-level difference between male and female knockout mice is consistent with the near complete absence of differences at the single cell level.

Discussion

For the present study, we examined male and female mice with PTEN deleted from ≈27% of their hippocampal granule cells. We have previously demonstrated that these mice develop epilepsy. Here, we explored potential mechanisms of epileptogenesis in these animals by assessing the morphology and physiology of their PTEN KO cells. PTEN KO cells developed a tendency to fire doublets and triplets, suggestive of increased intrinsic excitability, and received more spontaneous excitatory postsynaptic currents (sEPSCs) and fewer inhibitory currents (sIPSCs), indicating that the network the PTEN KO cells are embedded in has changed. Concomitant with these physiological changes, PTEN knockout cells developed longer dendrites with more branches, however, dendritic trees showed impaired self-avoidance, resulting in overlapping dendritic branches. Finally, we compared these physiological and morphological features between male and female mice. Cells from females (both control and KOs) received more sEPSCs and sIPSCs, demonstrating a clear dimorphism, but no net functional change; at least as assessed by sEPSC/sIPSC ratios and population responses to stimulation in slices. Interestingly, evoked spikes in KO cells from male mice occurred at lower frequencies than KO cells from female mice, demonstrating that subtle sex differences are present. Together, these findings reveal changes among single, PTEN KO granule cells likely to promote hyperexcitability in both male and female mice.

PTEN KO cells show altered intrinsic excitability

Whole cell voltage clamp recordings from individual PTEN-KO cells revealed significant changes in membrane parameters. Consistent with prior studies (Luikart et al., 2011; Weston et al., 2014; Williams et al., 2015), PTEN KO cells had lower input resistance. By contrast,

however, action potentials were elicited at similar membrane potentials using the present PTEN KO model, while KO cells fired at more hyperpolarized membrane potentials in the retroviral-Cre model used by Williams and colleagues (2015). This difference may be related to the methodology used to determine membrane parameters. While we derived the values under voltage clamp, Williams and colleagues obtained theirs under current clamp. Under voltage clamp condition, the rate of the ramp (140 mV sec^{-1} in our case) will influence the values of the activation potential of the spike, however, the effects of membrane capacitance, which affects the charging of the membrane, and membrane resistance, which alters the change in voltage per unit current (following injection of a current step) are negated. The activation potential that we obtained for the spike current is similar between the control and KO cells suggesting that 1) the molecular structure of the Na channel has not changed as a result of the deletion of PTEN, and 2) the site of generation of the action potential is close to the soma since the voltage control is adequate despite the large soma size of the KO cells.

Interestingly, many of the KO cells showed a tendency to fire action potential doublets or triplets at the beginning of the ramp. This tendency towards burst firing is remarkably similar to the appearance of evoked doublets among granule cells in the pilocarpine model of epilepsy (Pierce et al., 2011; Cameron et al., 2011; Althaus et al., 2015; Kelly and Beck, 2016). Although the animals in these studies were genetically normal, pilocarpine status epilepticus produces a prolonged increase in mTOR signaling (Zeng et al., 2009; Gorter et al., 2014), suggesting a potential molecular mechanism for the change. In addition, KO cells have a higher frequency of spikes generated per ramp as compared to control cells. The ability to fire doublets or triplets – coupled with a higher number of action potentials generated – point to an increased excitability

that could be an underlying mechanism by which KO cells enhance abnormal evoked circuit responses.

PTEN KO cells have impaired excitation/inhibition balance

A key finding of the present study is that KO granule cell receive more spontaneous excitatory input, and less spontaneous inhibitory input. A number of studies have described increased sEPSC (Luikart et al., 2011) and miniature EPSC (Luikart et al., 2011; Haws et al., 2014; Williams et al., 2015) frequency among PTEN KO granule cells. In contrast with the present study, however, Luikart and colleagues (2011) found no change in sIPSC or mIPSC frequency. Notably, since animals in the present model were epileptic, changes in IPSCs could reflect secondary epileptogenic changes, rather than direct effects of PTEN loss. Work by Weston and colleagues (2012; 2014) using a reductionist single-cell culture system revealed similar mEPSC and mIPSC frequencies in KO and control hippocampal neurons, favoring the interpretation that the changes observed here reflect secondary effects. Future work will be needed to dissociate primary from secondary changes, but the present findings suggest that reduced inhibitory input could be an important part of an epileptogenic cascade in the PTEN model.

Increased sEPSC frequency could reflect greater activity among excitatory afferents, higher release probabilities, greater numbers of afferents or some combination thereof. Our prior work in this model (Pun et al., 2012) and work by other investigators in related PTEN KO models (Kwon et al., 2006; Zhou et al., 2009; Luikart et al., 2011) consistently demonstrates increased dendritic spine density among KO granule cells. Dendritic spines are the key

postsynaptic structure receiving excitatory inputs, so increased spine density favors the interpretation that higher sEPSC frequency reflects greater numbers of inputs. Larger apical dendrites and the addition of basal dendrites – typically absent from control granule cells – further increases the area for afferent innervation. Modeling of these changes by Williams and colleagues (2015) revealed that increased input likely reflects a combination of these dendritic changes, plus an increase in EPSC amplitude. Reduced sIPSC frequency, on the other hand, could reflect fewer inhibitory inputs, reduced activity of inhibitory afferents or outright loss of inhibitory cells. Notably, the excitation/inhibition imbalance produced by PTEN deletion is reminiscent of that seen for hilar ectopic granule cells in the pilocarpine model of epilepsy (Zhan et al., 2010), again suggesting that such dysfunction could be mediated by enhanced mTOR signaling. The disruption in excitatory/inhibitory balance produced by the shift towards more EPSCs and fewer IPSCs provides an appealing explanation for the hyperactivity evident in these animals (Pun et al., 2012; LaSarge et al., 2016).

PTEN KO cell dendrites show impaired self-avoidance

Granule cells develop stereotypical, fanlike apical dendritic trees with dendrites spreading evenly in the molecular layer from their origin at the soma (Cajal, 1893; Rahimi and Claiborne, 2007). Secondary branches follow the same pattern, growing away from other branches belonging to the same cell. Evenly-spaced dendritic trees are hypothesized to improve the cells ability to sample incoming afferent inputs, in a fashion analogous to a tree in the forest spacing its branches in stereotypical fashion, so that leaves above do not block the sunlight for leaves below. The functional consequences of the “collapsed” dendritic trees evident in the present study are less, clear, but would be predicted to reduce granule cell sampling efficiency of

perforant path inputs. Convex hull analysis reveals that PTEN KO granule cells generate larger dendrites to sample the same volume of neuropil as control cells. This could create a relatively higher density of innervation, thereby increasing the efficacy of the input. Granule cells are hypothesized to by critical for pattern separation. Disrupted dendritic trees, therefore, may contribute to memory and cognitive deficits observed in PTEN KO animals (Kwon et al., 2006; Amiri et al., 2012; Lugo et al., 2014).

PTEN is a known regulator of dendritic growth (Chow et al., 2009), and protocadherins are implicated in regulating dendrite self-avoidance (Hayashi and Takeichi, 2015). The specific molecules that regulate dendrite self-avoidance in granule cells, however, have yet to be elucidated. Potential mechanisms by which mTOR might act, therefore, remain speculative. Nevertheless, the robust disruption of dendrite self-avoidance in PTEN KO cells strongly suggest the pathway in involved.

Intriguingly, impaired dendritic self-avoidance among granule cells is not unique to the PTEN model. Disrupted granule cell dendritic trees were noted in the 1970s in tissue collected from epilepsy surgeries. Granule cells in the resected tissue exhibited abnormalities highly reminiscent of these observed here, described as a “closed parasol” deformation (Scheibel and Scheibel, 1973). Later studies have described similar abnormalities among granule cells in the rodent pilocarpine model of epilepsy (Walter et al 2007; Kron et al 2010; Murphy et al 2011; Santos et al 2011). mTOR signaling is significantly increased during epileptogenesis in this model, raising the possibility that mTOR hyperactivation disrupts granule cell dendritic patterning in acquired epilepsies too.

Sexual dimorphism in excitatory/inhibitory inputs

Physiological studies revealed that granule cells from female animals received more excitatory and inhibitory input than males. The differences were evident in both control and KO cells, indicating that the dimorphism is a natural property of the cells, and not specific to PTEN deletion. There is precedent for the observation, with work by Woolley and colleagues showing sex differences in the mechanisms by which estradiol regulates both glutamatergic (Oberlander and Woolley, 2016) and GABAergic (Huang and Woolley, 2012; Tabatadze et al., 2015) transmission of hippocampal CA1 pyramidal cells. Although less extensively studied, estradiol has also been found to regulate granule cell spine density (Miranda et al., 1999; Bender et al., 2010; Hojo et al., 2015). Sex differences are well-established for many epilepsy disorders and it is hypothesized that underlying differences in neurotransmission, at least in part, account for the effect (Galanopoulou, 2014; Scharfman and MacLusky, 2014). One limitation of the present study is that the estrous cycle phase was not determined for female mice. Although no differences in field potential responses were found between males and females in the present study, and gross differences in seizure phenotype were not evident in past work with this model (Pun et al., 2012), future studies – categorizing females by the estrous phase – could reveal differences. Interictal spike frequency, for example, has been shown to vary with the estrous cycle phase in the kainic acid model of epilepsy (D'Amour et al., 2015), and this is therefore a promising target.

Conclusions

Hyperactivation of the mTOR pathway, via PTEN deletion or a variety of other mechanisms, is associated with a diverse set of neurological diseases (Crino, 2016). The exact mechanisms by which excess mTOR signaling promotes disease, however, remains uncertain. Here, we demonstrate that PTEN deletion represents a double-threat to granule cells; simultaneously increasing excitatory input while decreasing inhibitory control. PTEN loss also produces profound disruptions of the granule cell dendritic tree, likely further altering excitability and impairing normal hippocampal function. Lastly, we observe that these morphological and physiological changes are highly reminiscent of changes seen in acquired epilepsy. Changes in the PTEN model occur in the absence of widespread neuronal loss evident in many acquired epilepsy models (Borges et al., 2003; Castro et al., 2011), suggesting that mTOR signaling maybe a common node of disruption in epilepsy.

Figure Legends

Figure 1: Confocal optical sections of the dentate gyrus showing PTEN (**A**, red) and Nissl staining (**B**, blue) in male and female PTEN KO mice. PTEN KO cells are evident as "holes" in the granule cell layer in the PTEN images, and as blue, Nissl-stained cells in the merged image (**C**). The percentage of PTEN KO granule cells was statistically identical between males and females. Scale = 50 µm. **D:** Confocal maximum projections of biocytin-filled granule cells from male and female mice showing knockout cells (*) with enlarged somas, and adjacent PTEN-expressing ($PTEN^{+/+}$) cells. Scale = 50 µm. **E:** PTEN immunostaining was unreliable in thick sections used for physiology, so soma area was used as a surrogate marker for PTEN KO cells. To validate this approach, the soma areas of $PTEN^{+/+}$ cells from wild type (WT) mice (grey and pink columns), $PTEN^{+/+}$ cells from PTEN KO mice (white columns with black or red edges), and $PTEN^{-/-}$ cells from PTEN KO mice (black and red columns) were measured. Graphs show negligible overlap between the soma areas of $PTEN^{+/+}$ and PTEN KO cells. Red bars denote two standard deviations of the mean. Note that soma areas shown in figure 1 are smaller than areas for biocytin-filled cells due to shrinkage artifact from dehydration and xylene clearing.

Figure 2, A: PTEN KO cells fire doublets and triplets at the beginning of a voltage ramp (-100 to +40 mV). Representative traces from cells from male and female control and knockout mice are shown. Arrows denote triplets from KO cells. Calibration = 200 pA, 0.2 sec. **B:** KO cells from male mice exhibit longer inter-spike intervals than cells from male controls during ramp firing. Doublets and triplets were excluded from this analysis. ***, $p<0.001$, KO vs. control

within male. **C:** KO cells fire more spikes per voltage ramp than control cells. **, p<0.01, main effect, KO vs. control.

Figure 3: PTEN KO cells from both male and female mice show increased sEPSC frequency (**A**), and decreased sIPSC frequency (**B**) relative to sex-matched controls (genotype effects noted by brackets: {)**.** In addition, female mice exhibited more sEPSCs and sIPSCs than males (sex effects noted by bars). **C:** sEPSC/IPSC ratios increased significantly for knockout cells vs. controls. No sex difference in sEPSC/IPSC ratios, however, was evident. *, p<0.05; **, p<0.01; ***, p<0.001; two-way ANOVA. Representative traces for each cell type are shown. Calibration bar: 2 pA, 0.5 sec. Controls are depicted by grey and pink bars, and KOs by black and red.

Figure 4: Neuronal reconstructions from confocal image z-stacks (top row) and Neurolucida reconstructions (line drawings) of PTEN KO hippocampal granule cells from male and female control and knockout mice. Scale bar = 100 μm.

Figure 5: Quantification of granule cell dendrite length and branch nodes. Measurements are provided for the whole cell (total) and broken down by dendritic segments contained within the granule cell layer (DGC-L), and inner (IML), middle (MML) and outer (OML) molecular layers. Bar graphs are used for parametric data, and box plots for non-parametric data. *, p<0.05, main effect of genotype. ***, p<0.001; main effect of genotype.

Figure 6: Images show granule cell reconstructions viewed from the top (left, cells A-D), looking down from the top of the dendritic tree towards the soma, and then the same cells viewed

in profile (right, a-d). Note the more limited spread of the dendritic tree, and frequent overlapping dendrites. Reconstructions are color-coded by depth. Scale bars = 100 μm. ***, $p<0.001$; main effect of genotype.

Figure 7, A: PTEN KO granule cells exhibit a failure of dendrite self-avoidance, which was quantified using a dendritic overlap index; defined as the number of times dendrites crossed over each other in 2-dimensional projections. Higher values reflect greater overlap. **B:** Dendritic structure was also assessed using a 3D convex hull analysis, which revealed that the dendritic trees of cells from all four groups encompassed similar volumes. **C:** While entire dendritic trees encompassed similar volumes (B), individual primary dendrites of KO cells encompassed significantly smaller volumes than primary dendrites from control cells. **D:** A non-significant trend towards reduced 3D hull volume/micron of dendrite was also evident for KO cells. Bar graphs are used for parametric data, and box plots for non-parametric data. ***, $p<0.001$; *, $p<0.05$; main effect of genotype. **E:** Model detailing the graphical data. Green ovals represent the average 3D convex hull volume from control and KO cells, which were statistically similar among groups (B). Black ovals represent the average 3D convex hull volumes for primary dendrites making up the trees for control and KO cells. Volumes were smaller for KO cells (C). KO cell dendrites expand through the same volume of tissue, therefore, but achieve this using greater numbers of primary dendrites, resulting in smaller primary dendrite hull volume and more overlapping branches.

Figure 8: Field potential responses, recorded in the granule cell layer, are shown following stimulation of the perforant path at 6V. Responses were graded using a semi-quantitative 1-4 point scale. Examples of the four response categories, defined by the appearance of excitatory postsynaptic potentials (EPSPs) and population (pop.) spikes, are provided. The graph shows median responses in slices from male and female control and knockout mice. Scale for traces is 1 mV x 5 mS. ***, $p<0.001$.

References

Althaus AL, Sagher O, Parent JM, Murphy GG (2015) Intrinsic neurophysiological properties of hilar ectopic and normotopic dentate granule cells in human temporal lobe epilepsy and a rat model. J Neurophysiol. 113(4):1184-94.

Althaus AL, Zhang H, Parent JM (2016) Axonal plasticity of age-defined dentate granule cells in a rat model of mesial temporal lobe epilepsy. Neurobiol Dis. 86:187-96.

Amiri A, Cho W, Zhou J, Birnbaum SG, Sinton CM, McKay RM, Parada LF (2012) Pten deletion in adult hippocampal neural stem/progenitor cells causes cellular abnormalities and alters neurogenesis. J Neurosci. 32(17):5880-90.

Baar EL, Carbajal KA, Ong IM, Lamming DW (2016) Sex- and tissue-specific changes in mTOR signaling with age in C57BL/6J mice. Aging Cell. 15(1):155-66.

Bender RA, Zhou L, Wilkars W, Fester L, Lanowski JS, Paysen D, König A, Rune GM (2010) Roles of 17ß-estradiol involve regulation of reelin expression and synaptogenesis in the dentate gyrus. Cereb Cortex. 20(12):2985-95.

Borges K, Gearing M, McDermott DL, Smith AB, Almonte AG, Wainer BH, Dingledine R (2003) Neuronal and glial pathological changes during epileptogenesis in the mouse pilocarpine model. Exp Neurol. 182(1):21-34.

Butler CR, Boychuk JA, Smith BN (2015) Effects of Rapamycin Treatment on Neurogenesis and Synaptic Reorganization in the Dentate Gyrus after Controlled Cortical Impact Injury in Mice. Front Syst Neurosci. 9:163.

Cameron MC, Zhan RZ, Nadler JV (2011) Morphologic integration of hilar ectopic granule cells into dentate gyrus circuitry in the pilocarpine model of temporal lobe epilepsy. J Comp Neurol. 519(11):2175-92.

Castro OW, Furtado MA, Tilelli CQ, Fernandes A, Pajolla GP, Garcia-Cairasco N (2011) Comparative neuroanatomical and temporal characterization of FluoroJade-positive neurodegeneration after status epilepticus induced by systemic and intrahippocampal pilocarpine in Wistar rats. Brain Res. 1374:43-55.

Chow DK, Groszer M, Pribadi M, Machniki M, Carmichael ST, Liu X, Trachtenberg JT (2009) Laminar and compartmental regulation of dendritic growth in mature cortex. Nat Neurosci. 12(2):116-8.

Crino PB (2016) The mTOR signaling cascade: paving new roads to cure neurological disease. Nat Rev Neurol. 12(7):379-92.

Cho KO, Lybrand ZR, Ito N, Brulet R, Tafacory F, Zhang L, Good L, Ure K, Kernie SG, Birnbaum SG, Scharfman HE, Eisch AJ, Hsieh J. (2015) Aberrant hippocampal neurogenesis contributes to epilepsy and associated cognitive decline. Nat Commun. 6:6606.

D'Amour J, Magagna-Poveda A, Moretto J, Friedman D, LaFrancois JJ, Pearce P, Fenton AA, MacLusky NJ, Scharfman HE (2015) Interictal spike frequency varies with ovarian cycle stage in a rat model of epilepsy. Exp Neurol. 269:102-19.

Danzer SC, Pan E, Nef S, Parada LF, McNamara JO (2004) Altered regulation of BDNF protein in hippocampus following slice preparation. Neuroscience 126:859–869.

Deller T, Drakew A, Frotscher M (1999) Different primary target cells are important for fiber lamination in the fascia dentata: a lesson from reeler mutant mice. Exp Neurol 156:239 –253.

Galanopoulou AS (2014) Sex and epileptogenesis, introduction to the special issue. Neurobiol Dis. 72 Pt B:123-4.

Garcia-Junco-Clemente P, Golshani P (2014) PTEN: A master regulator of neuronal structure, function, and plasticity. Commun Integr Biol. 7(1):e28358.

Gorter JA, Iyer A, White I, Colzi A, van Vliet EA, Sisodiya S, Aronica E (2014) Hippocampal subregion-specific microRNA expression during epileptogenesis in experimental temporal lobe epilepsy. Neurobiol Dis. 62:508-20.

Gürgen D, Kusch A, Klewitz R, Hoff U, Catar R, Hegner B, Kintscher U, Luft FC, Dragun D (2013) Sex-specific mTOR signaling determines sexual dimorphism in myocardial adaptation in normotensive DOCA-salt model. Hypertension 61(3):730-6.

Haws ME, Jaramillo TC, Espinosa F, Widman AJ, Stuber GD, Sparta DR, Tye KM, Russo SJ, Parada LF, Stavarache M, Kaplitt M, Bonci A, Powell CM (2014) PTEN knockdown alters dendritic spine/protrusion morphology, not density. J Comp Neurol. 522(5):1171-90.

Hayashi S, Takeichi M (2015) Emerging roles of protocadherins: from self-avoidance to enhancement of motility. J Cell Sci. 128(8):1455-64.

Heng K, Haney MM, Buckmaster PS (2013) High-dose rapamycin blocks mossy fiber sprouting but not seizures in a mouse model of temporal lobe epilepsy. Epilepsia 54(9):1535-41.

Hojo Y, Munetomo A, Mukai H, Ikeda M, Sato R, Hatanaka Y, Murakami G, Komatsuzaki Y, Kimoto T, Kawato S (2015) Estradiol rapidly modulates spinogenesis in hippocampal dentate gyrus: Involvement of kinase networks. Horm Behav. 74:149-56.

Hosford BE, JP Liska, SC Danzer (2016) Ablation of Newly-generated Hippocampal Granule Cells has Disease-Modifying Effects in Epilepsy. Journal of Neuroscience, 36(43):11013-11023.

Huang GZ, Woolley CS (2012) Estradiol acutely suppresses inhibition in the hippocampus through a sex-specific endocannabinoid and mGluR-dependent mechanism. Neuron 74(5):801-8.

Huang X, Zhang H, Yang J, Wu J, McMahon J, Lin Y, Cao Z, Gruenthal M, Huang Y. (2010) Pharmacological inhibition of the mammalian target of rapamycin pathway suppresses acquired epilepsy. Neurobiol Dis. 40(1):193-9.

Jansen LA, Mirzaa GM, Ishak GE, O'Roak BJ, Hiatt JB, Roden WH, Gunter SA, Christian SL, Collins S, Adams C, Rivière JB, St-Onge J, Ojemann JG, Shendure J, Hevner RF, Dobyns WB (2015) PI3K/AKT pathway mutations cause a spectrum of brain malformations from megalencephaly to focal cortical dysplasia. Brain 138(Pt 6):1613-28.

Jessberger S, Parent JM (2015) Epilepsy and Adult Neurogenesis. Cold Spring Harb Perspect Biol. 2015 Nov 9;7(12).

Jones RSG, Heinemann U (1988) Synaptic and Intrinsic Responses of Medial Endorhinal Cortical Cells in Normal and Magnesium-Free Medium In Vitro. J. Neurophysiol. 59 (5): 1476-96.

Kelly T, Beck H (2017) Functional properties of granule cells with hilar basal dendrites in the epileptic dentate gyrus. Epilepsia 58(1):160-171.

Kron MM1, Zhang H, Parent JM (2010) The developmental stage of dentate granule cells dictates their contribution to seizure-induced plasticity. J Neurosci. 30(6):2051-9.

Krook-Magnuson E, Armstrong C, Bui A, Lew S, Oijala M, Soltesz I (2015) In vivo evaluation of the dentate gate theory in epilepsy. J Physiol. 593(10):2379-88.

Kwon CH, Zhu X, Zhang J, Knoop LL, Tharp R, Smeyne RJ, Eberhart CG, Burger PC, Baker SJ (2001) Pten regulates neuronal soma size: a mouse model of Lhermitte-Duclos disease. Nat Genet. 29(4):404-11.

Kwon CH, Zhu X, Zhang J, Baker SJ (2003) mTor is required for hypertrophy of Pten-deficient neuronal soma in vivo. Proc Natl Acad Sci U S A. 100(22):12923-8.

Kwon CH, Luikart BW, Powell CM, Zhou J, Matheny SA, Zhang W, Li Y, Baker SJ, Parada LF (2006) Pten regulates neuronal arborization and social interaction in mice. Neuron 50(3):377-88.

LaSarge CL, Danzer SC (2014) Mechanisms regulating neuronal excitability and seizure development following mTOR pathway hyperactivation. Front Mol Neurosci. 7:18.

LaSarge CL, Santos VR, Danzer SC (2015) PTEN deletion from adult-generated dentate granule cells disrupts granule cell mossy fiber axon structure. Neurobiol Dis. 75:142-50.

LaSarge CL, Pun RY, Muntifering MB, Danzer SC (2016) Disrupted hippocampal network physiology following PTEN deletion from newborn dentate granule cells. Neurobiol Dis. 96:105-114.

Lipton JO, Sahin M, (2014) The neurology of mTOR. Neuron 84(2):275-291.

Ljungberg MC, Sunnen CN, Lugo JN, Anderson AE, D'Arcangelo G (2009) Rapamycin suppresses seizures and neuronal hypertrophy in a mouse model of cortical dysplasia. Dis Model Mech. 2(7-8):389-98.

Lugo JN, Smith GD, Arbuckle EP, White J, Holley AJ, Floruta CM, Ahmed N, Gomez MC, Okonkwo O (2014) Deletion of PTEN produces autism-like behavioral deficits and alterations in synaptic proteins. Front Mol Neurosci. 7:27.

Luikart BW, Schnell E, Washburn EK, Bensen AL, Tovar KR, Westbrook GL (2011) Pten knockdown in vivo increases excitatory drive onto dentate granule cells. J Neurosci. 31(11):4345-54.

Matsushita Y, Sakai Y, Shimmura M, Shigeto H, Nishio M, Akamine S, Sanefuji M, Ishizaki Y, Torisu H, Nakabeppu Y, Suzuki A, Takada H, Hara T (2016) Hyperactive mTOR signals in the proopiomelanocortin-expressing hippocampal neurons cause age-dependent epilepsy and premature death in mice. Sci Rep. 6:22991.

McAuliffe JJ, Bronson SL, Hester MS, Murphy BL, Dahlquist-Topalá R, Richards DA, Danzer SC (2011) Altered patterning of dentate granule cell mossy fiber inputs onto CA3 pyramidal cells in limbic epilepsy. Hippocampus 21(1):93-107.

Miller RA, Harrison DE, Astle CM, Fernandez E, Flurkey K, Han M, Javors MA, Li X, Nadon NL, Nelson JF, Pletcher S, Salmon AB, Sharp ZD, Van Roekel S, Winkleman L, Strong R (2014) Rapamycin-mediated lifespan increase in mice is dose and sex dependent and metabolically distinct from dietary restriction. Aging Cell. 13(3):468-77.

Miranda P, Williams CL, Einstein G (1999) Granule cells in aging rats are sexually dimorphic in their response to estradiol. J Neurosci. 19(9):3316-25.

Murphy BL, Pun RY, Yin H, Faulkner CR, Loepke AW, Danzer SC (2011) Heterogeneous integration of adult-generated granule cells into the epileptic brain. J Neurosci. 31(1):105-17.

Murphy BL, Hofacer RD, Faulkner CN, Loepke AW and SC Danzer (2012) Abnormalities of granule cell dendritic structure are a prominent feature of the intrahippocampal kainic acid model of epilepsy despite reduced post-injury neurogenesis. Epilepsia 53 (5):908-921.

Nguyen LH, Brewster AL, Clark ME, Regnier-Golanov A, Sunnen CN, Patil VV, D'Arcangelo G, Anderson AE (2015) mTOR inhibition suppresses established epilepsy in a mouse model of cortical dysplasia. Epilepsia 56(4):636-46.

Oberlander JG, Woolley CS (2016) 17β-Estradiol Acutely Potentiates Glutamatergic Synaptic Transmission in the Hippocampus through Distinct Mechanisms in Males and Females. J Neurosci. 36(9):2677-90.

O'Roak BJ, Vives L, Fu W, Egertson JD, Stanaway IB, Phelps IG, Carvill G, Kumar A, Lee C, Ankenman K, Munson J, Hiatt JB, Turner EH, Levy R, O'Day DR, Krumm N, Coe BP, Martin BK, Borenstein E, Nickerson DA, Mefford HC, Doherty D, Akey JM, Bernier R, Eichler EE, Shendure J (2012) Multiplex targeted sequencing identifies recurrently mutated genes in autism spectrum disorders. Science 338(6114):1619-22.

Pierce JP, McCloskey DP, Scharfman HE (2011) Morphometry of hilar ectopic granule cells in the rat. J Comp Neurol. 519(6):1196-218.

Pun RY, Kleene SJ (2003) Contribution of cyclic-nucleotide-gated channels to the resting conductance of olfactory receptor neurons. Biophys J. 84(5):3425-35.

Pun RY, Kleene SJ (2004) An estimate of the resting membrane resistance of frog olfactory receptor neurones. J Physiol. 559(Pt 2):535-42.

Pun RY, Rolle IJ, Lasarge CL, Hosford BE, Rosen JM, Uhl JD, Schmeltzer SN, Faulkner C, Bronson SL, Murphy BL, Richards DA, Holland KD, Danzer SC (2012) Excessive activation of mTOR in postnatally generated granule cells is sufficient to cause epilepsy. Neuron 75(6):1022-1034.

Paxinos, G., Franklin, K. B. J. (2001) The Mouse Brain in Stereotaxic Coordinates. Academic Press, San Diego.

Rahimi O, Claiborne BJ (2007) Morphological development and maturation of granule neuron dendrites in the rat dentate gyrus. Prog Brain Res. 163:167-81.

Ramón y Cajal, S.R. (1893) Estructura del asta de Ammon. Anal. Soc. Esp. Hist. Nat. (Madrid), 22:53–114.

Reddy DS (2017) The neuroendocrine basis of sex differences in epilepsy. Pharmacol Biochem Behav. 152:97-104.

Santos VR, de Castro OW, Pun RY, Hester MS, Murphy BL, Loepke AW, Garcia-Cairasco N, Danzer SC (2011) Contributions of mature granule cells to structural plasticity in temporal lobe epilepsy. Neuroscience 197:348-57.

Scharfman HE, MacLusky NJ (2014) Sex differences in the neurobiology of epilepsy: a preclinical perspective. Neurobiol Dis. 72 Pt B:180-92.

Scharfman HE, Bernstein HL (2015) Potential implications of a monosynaptic pathway from mossy cells to adult-born granule cells of the dentate gyrus. Front Syst Neurosci. 9:112.

Scheibel ME, Scheibel AB (1973) Hippocampal pathology in temporal lobe epilepsy: a Golgi survey. In: Epilepsy: its phenomena in man (Brazier MAB, Ed.). London: Academic.

Shapiro LA, Upadhyaya P, Ribak CE. (2007) Spatiotemporal profile of dendritic outgrowth from newly born granule cells in the adult rat dentate gyrus. Brain Res. 1149:30-7.

Singh SP, LaSarge CL, An A, McAuliffe JJ, Danzer SC (2016) Clonal Analysis of Newborn Hippocampal Dentate Granule Cell Proliferation and Development in Temporal Lobe Epilepsy. eNeuro. 2(6).

Switon K, Kotulska K, Janusz-Kaminska A, Zmorzynska J, Jaworski J (2017) Molecular neurobiology of mTOR. Neuroscience 341:112-153.

Tabatadze N, Huang G, May RM, Jain A, Woolley CS (2015) Sex Differences in Molecular Signaling at Inhibitory Synapses in the Hippocampus. J Neurosci. 35(32):11252-65.

Takeuchi K, Gertner MJ, Zhou J, Parada LF, Bennett MV, Zukin RS (2013) Dysregulation of synaptic plasticity precedes appearance of morphological defects in a Pten conditional knockout mouse model of autism. Proc Natl Acad Sci U S A. 110(12):4738-43.

Thome C, Kelly T, Yanez A, Schultz C, Engelhardt M, Cambridge SB, Both M, Draguhn A, Beck H, Egorov AV (2014) Axon-carrying dendrites convey privileged synaptic input in hippocampal neurons. Neuron 83(6):1418-30.

van Groen T, Miettinen P, Kadish I (2003) The entorhinal cortex of the mouse: organization of the projection to the hippocampal formation. Hippocampus 13:133–149.

Walter C, Murphy BL, Pun RY, Spieles-Engemann AL, Danzer SC (2007) Pilocarpine-induced seizures cause selective time-dependent changes to adult-generated hippocampal dentate granule cells. J Neurosci. 27(28):7541-52.

West MJ, Andersen AH (1980) An allometric study of the area dentata in the rat and mouse. Brain Res 2:317–348.

Weston MC, Chen H, Swann JW (2012) Multiple roles for mammalian target of rapamycin signaling in both glutamatergic and GABAergic synaptic transmission. J Neurosci. 32(33):11441-52.

Weston MC, Chen H, Swann JW (2014) Loss of mTOR repressors Tsc1 or Pten has divergent effects on excitatory and inhibitory synaptic transmission in single hippocampal neuron cultures. Front Mol Neurosci. 7:1.

Williams MR, DeSpenza T Jr, Li M, Gulledge AT, Luikart BW (2015) Hyperactivity of newborn Pten knock-out neurons results from increased excitatory synaptic drive. J Neurosci. 35(3):943-59.

Wong M, Moss RL (1992) Long-term and short-term electrophysiological effects of estrogen on the synaptic properties of hippocampal CA1 neurons. J Neurosci. 12(8):3217-25.

Zeng LH, Rensing NR, Wong M (2009) The mammalian target of rapamycin signaling pathway mediates epileptogenesis in a model of temporal lobe epilepsy. J Neurosci. 29(21):6964-72.

Zhao S, Ting JT, Atallah HE, Qiu L, Tan J, Gloss B, Augustine GJ, Deisseroth K, Luo M, Graybiel AM, Feng G (2011) Cell type-specific channelrhodopsin-2 transgenic mice for optogenetic dissection of neural circuitry function. Nat Methods 8: 745–752.

Zhan RZ, Timofeeva O, Nadler JV (2010) High ratio of synaptic excitation to synaptic inhibition in hilar ectopic granule cells of pilocarpine-treated rats. J Neurophysiol. 104(6):3293-3304.

Zhou J, Blundell J, Ogawa S, Kwon CH, Zhang W, Sinton C, Powell CM, Parada LF (2009) Pharmacological inhibition of mTORC1 suppresses anatomical, cellular, and behavioral abnormalities in neural-specific Pten knock-out mice. J Neurosci. 29(6):1773-83.

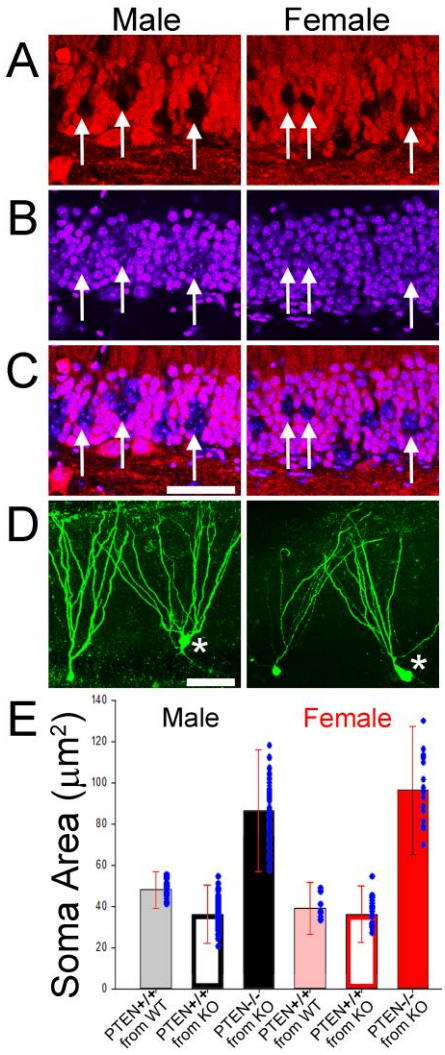

Fig. 1

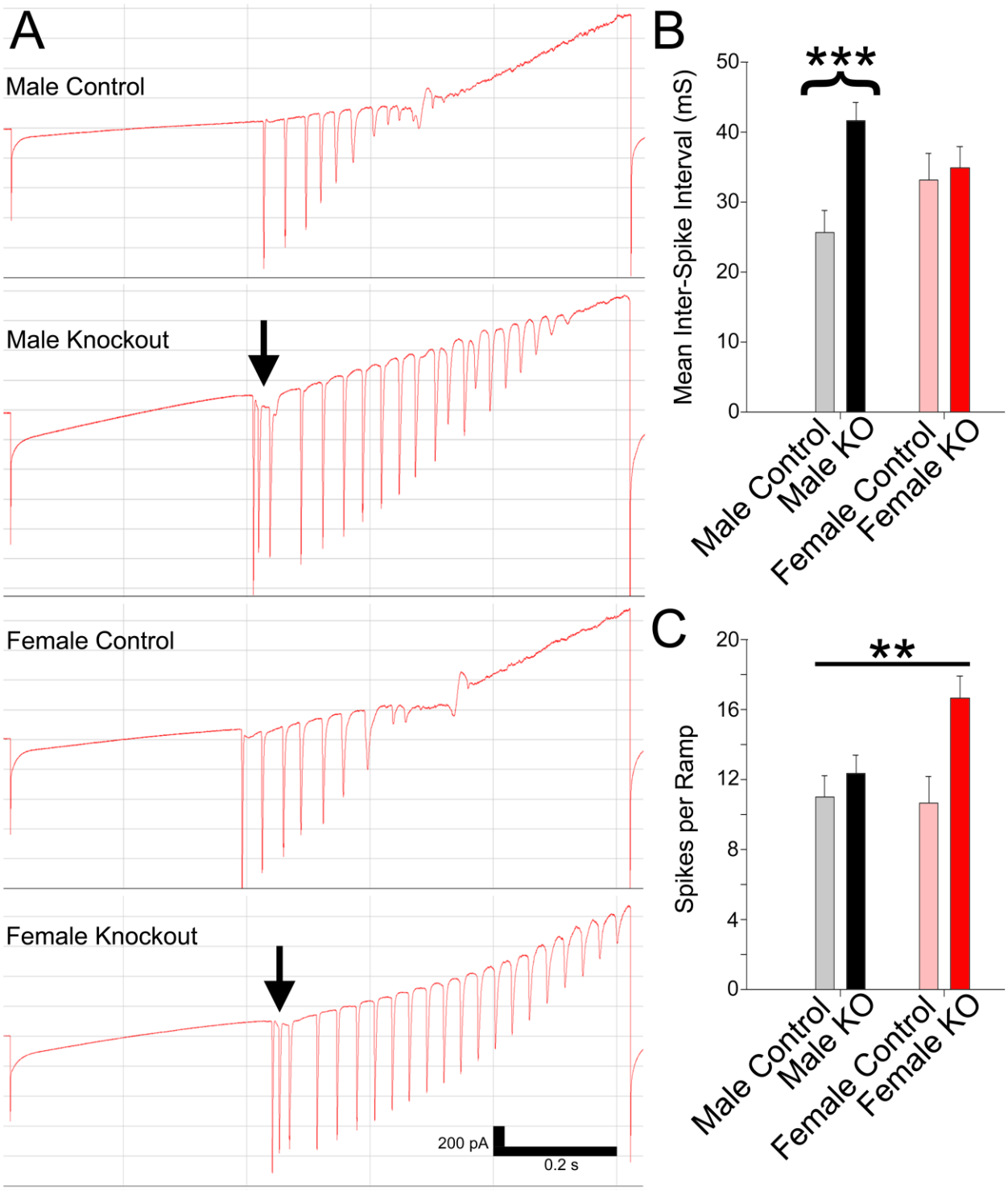

Fig. 2

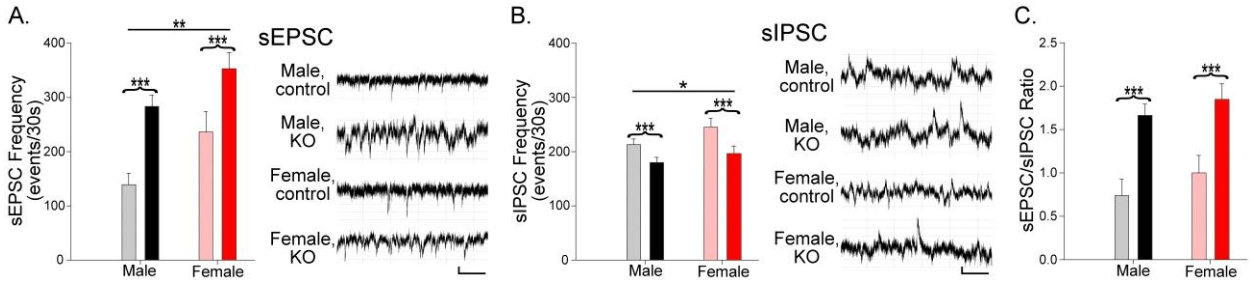

Fig. 3

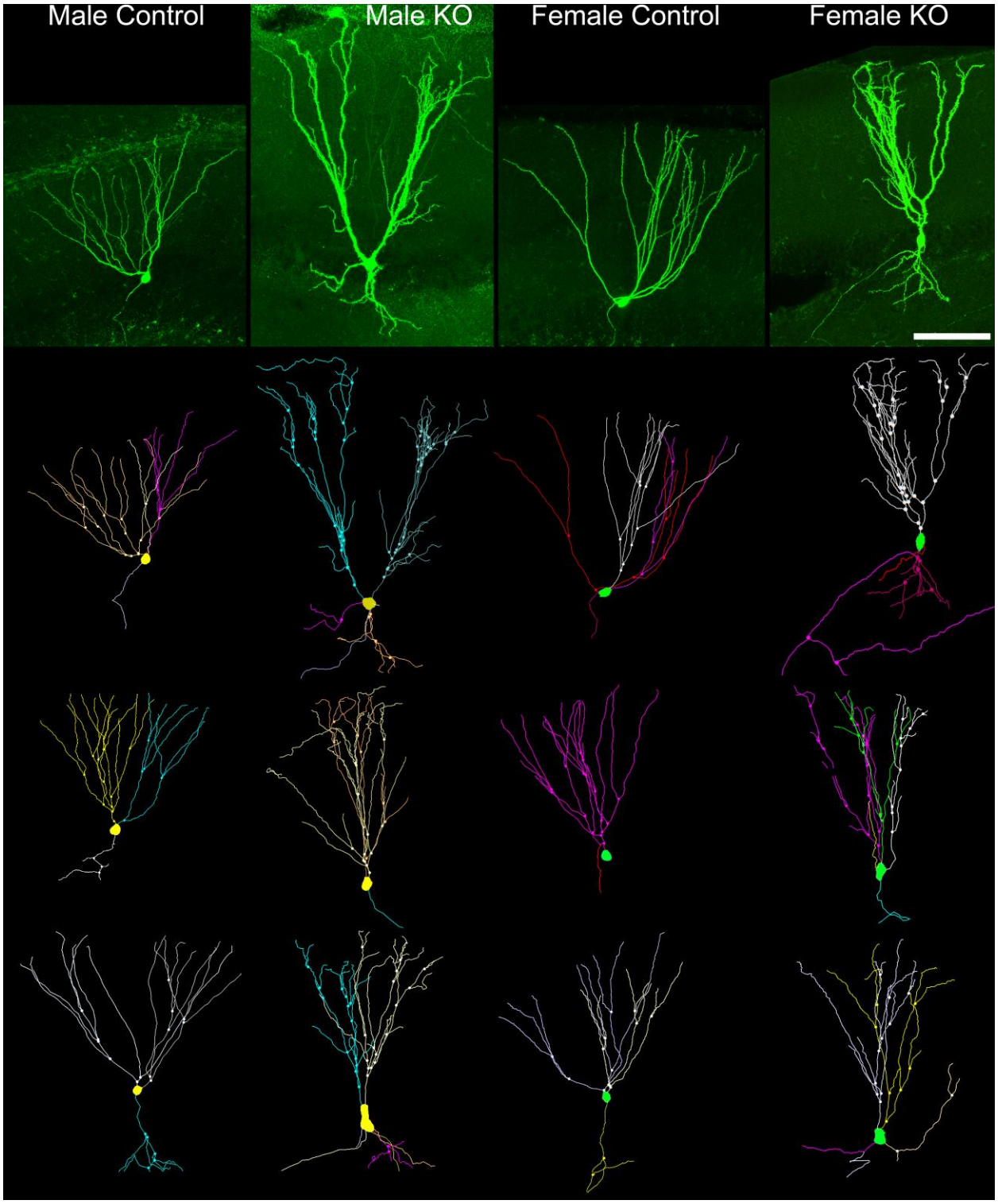

Fig. 4

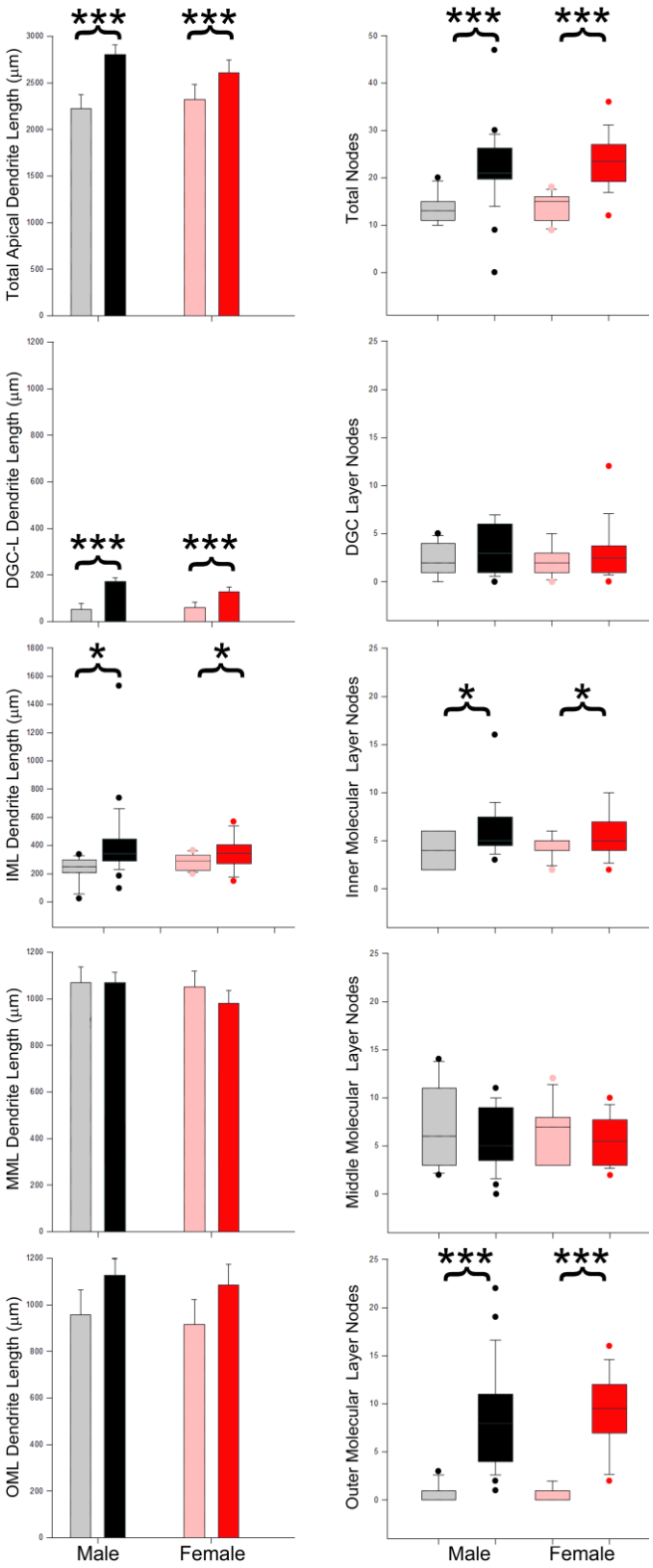

Fig. 5

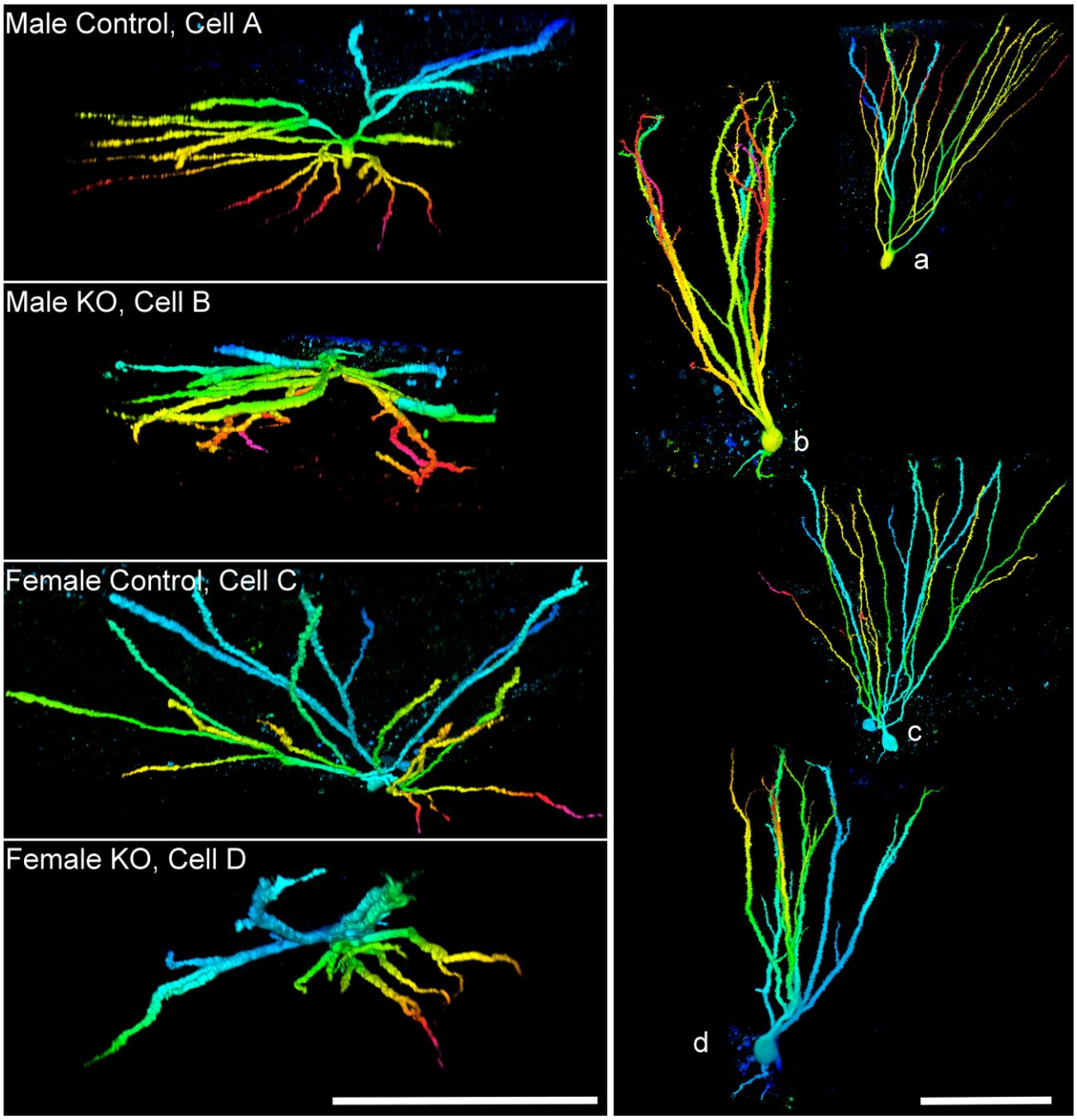

Fig. 6

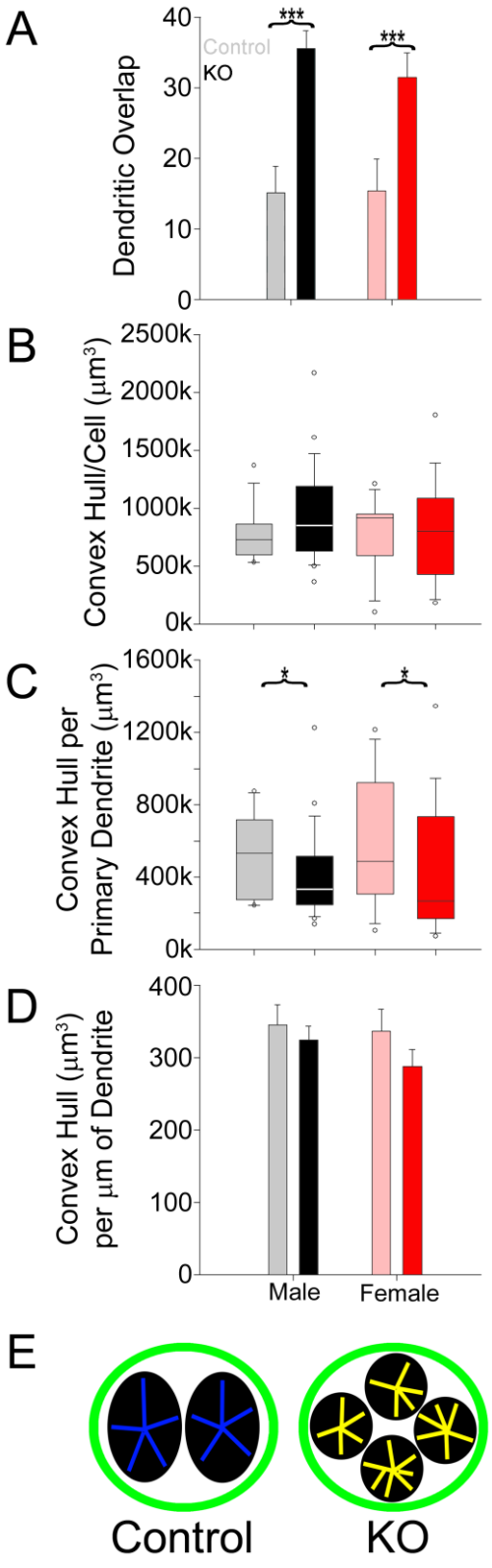

Fig. 7

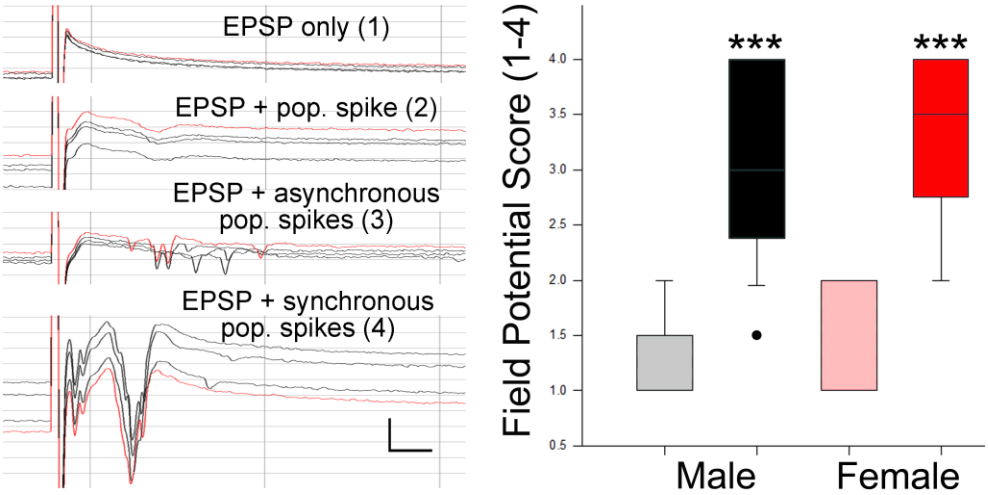

Fig. 8

Highlights

1. PTEN deletion increases excitatory input and decreases inhibitory input
2. PTEN deletion disrupts dendrite self-avoidance
3. Granule cells from females receive more input than cells from males
4. PTEN deletion increases inter-spike intervals in males, but not females